Nuclear Medicine and Biology 86-87 (2020) 59–65

Contents lists available at ScienceDirect

Nuclear Medicine and Biology

journal homepage: www.elsevier.com/locate/nucmedbio

EXIRAD-3D: Fast automated three-dimensional autoradiography

Minh Phuong Nguyen [a,*], Ruud M. Ramakers [a,b,c], Chris Kamphuis [b,c], Sofia Koustoulidou [b,c,d], Marlies C. Goorden [a], Freek J. Beekman [a,b,c]

[a] Section Biomedical Imaging, Delft University of Technology, Delft, the Netherlands
[b] MILabs B.V., Utrecht, the Netherlands
[c] Department of Translational Neuroscience, Brain Center Rudolf Magnus, University Medical Center Utrecht, the Netherlands
[d] Department of Radiology and Nuclear Medicine, Erasmus MC, 3015 CN, Rotterdam, the Netherlands

ARTICLE INFO

Article history:
Received 21 February 2020
Received in revised form 15 May 2020
Accepted 2 June 2020

Keywords:
Autoradiography
Pinhole
SPECT
Ex vivo
Molecular imaging

ABSTRACT

Introduction: Autoradiography is an established technique for high-resolution imaging of radiolabelled molecules in biological tissue slices. Unfortunately, creating a 3D image from a set of these 2D images is extremely time-consuming and error-prone. MicroSPECT systems provide such 3D images but have a low resolution. Here we present EXIRAD-3D, a fast automated method as an alternative for 3D autoradiography from coupes based on ultra-high resolution microSPECT technology.
Methods: EXIRAD-3D uses a very small bore focusing multi-pinhole collimator mounted in a SPECT system with stationary detectors (U-SPECT/CT, MILabs B.V. The Netherlands) using a sample holder with integrated tissue cooling to avoid activity leaking or tissue deformation during the scan. The system performance was experimentally evaluated using various phantoms and tissue samples of animals in vivo injected with technetium-99m and iodine-123.
Results: The reconstructed spatial resolution obtained with a Derenzo hot rod phantom was 120 μm (or 1.7 nl). The voxel values of a syringe phantom image appear to be uniform and scale linearly with activity. Uptake in tiny details of the mouse knee joint, thyroid, and kidney could be clearly visualized.
Conclusion: EXIRAD-3D opens up the possibility for fast and quantitative 3D imaging of radiolabelled molecules at a resolution far better than in vivo microSPECT and saves tremendous amounts of work compared to obtaining 3D data from a set of 2D autoradiographs.
Advances in knowledge and implications for patient care: EXIRAD-3D offers superior image resolution over microSPECT, and it can be a very efficient alternative for autoradiography in pharmaceutical and biological studies.

Data availability

The datasets generated during and/or analyzed during the current study are available from the corresponding author on reasonable request.

1. Introduction

Imaging of radiolabeled molecules in biological samples is key in pharmaceutical and biological research, e.g. to locally quantify drug distributions, to study metabolic pathways, or to localize enzymes and nucleic acids in cells. For resolutions below that of what can be achieved by in vivo PET and SPECT, these applications mainly rely on 2D autoradiography. Since its debut in the 1950s, autoradiography has gone through an extensive development process but is generally still based on the initial technique of tissue slicing [1,2]. Recent progress and current practice of autoradiography can be inferred from several review articles [3,4].

Traditional autoradiography has several limitations to be considered. It requires complex sample preparation and manipulation with sophisticated equipment and dedicated image analysis software. First, the tissue sample needs to be cryo-cooled, and sliced into thin sections using a cryo-microtome. Each section is then meticulously positioned on a phosphor imaging plate or a thin film pre-coated with a photographic emulsion, carefully tagged, and systematically arranged in light-tight and radioactivity-shielded boxes for imaging which typically lasts for days or sometimes even weeks [3]. The obtained 2D images can then be co-registered to form a 3D volume representing the radioactivity distribution within the sample – a process involving intensity correction, slice deformation and alignment by means of e.g. a principal-axes method, cross-correlation computation, and shape analysis [5–7]. The whole procedure is time-consuming and error-prone and potentially causes distortion and other artifacts in the obtained image volume,

* Corresponding author at: Mekelweg 15, 2629 JB Delft, the Netherlands.
E-mail address: m.p.nguyen@tudelft.nl (M.P. Nguyen).

https://doi.org/10.1016/j.nucmedbio.2020.06.001
0969-8051/

e.g. due to tears in the slices. Besides, since variability in the thickness of tissue sections and in the thickness of the detection media is often unavoidable, and because in common practice not all sections can be collected due to time limitations, labor and laboratory resources, 3D imaging with traditional autoradiography is still limited. Additionally, due to the long processing time, traditional autoradiography often utilizes long-lived isotopes (e.g. tritium (^{3}H), carbon-14 (^{14}C), phosphorus-32 (^{32}P), sulphur-35 (^{35}S), and iodine-125 (^{125}I)) but is less suitable for relatively short-lived isotopes (e.g. iodine-123 (^{123}I), technetium-99 m (^{99m}Tc), thallium-201 (^{201}Tl), and indium-111 (^{111}In)). It is of interest to investigate if another imaging modality can -at least for a subset of the applications- address these shortcomings and at the same time, also produce high-resolution images.

Alternative techniques have been developed to produce autoradiographs. Beta and Micro-Imagers (commercialized by Biospace Lab, Paris, France), utilizing a parallel plate avalanche chamber or scintillator sheet together with an image intensifier tube and charge-coupled-device (CCD) camera [8], are capable of fast multi-tracer quantitative imaging of radioactivity in tissues at high resolution. CCD technology has also been employed by other groups, either by directly converting particle energy into electric charge or by using scintillators [9–13]. These instruments have the drawback that only relatively few sections can be analyzed at the same time, and they do not directly produce 3D images. Aside from CCDs, various other detector types have been studied and realized as alternatives for traditional autoradiographic films and phosphor imaging plates, such as direct gaseous counters (BeaQuant, AI4R, Nantes, France), pixel array detectors [14–16], complementary metal-oxide-semiconductors [17,18], DEPFETs [19], silicon strip detectors [20], microchannel plates [21,22], and position-sensitive avalanche photodiodes [23]. In general, the systems with these detector types are not ready for fully 3D imaging either.

SPECT systems can produce 3D images of many radionuclides. However highest spatial resolution achieved with an in vivo preclinical pinhole SPECT modality in mice is now 0.25 mm (or 15.6 nl) [24], and about 0.7 mm in rats. It is extremely hard to push the resolution further due to the animal size which limits the pinhole magnification factor.

Since in ex vivo scans of biological tissue, the scanned object is smaller than in in vivo scanning, SPECT may reach a much better resolution: the pinholes' centers can be placed much closer to the object to increase both sensitivity and pinhole magnification. At the same time, if the tissue sample is frozen and a relatively long-lived isotope is used, a scan longer than typical in vivo SPECT scan times can be performed to acquire many counts. These characteristics together translate into a better image resolution as shown by [25] and [26]. This is the reason to investigate if ex vivo pinhole SPECT can operate in a resolutions range acceptable to replace at least some autoradiography applications.

For the reasons mentioned above, we developed an option for a SPECT system to enable fast automated 3D autoradiography. This was enabled by the development of a special narrow bore pinhole collimator combined with a cryo-cooled sample holder to keep the tissue frozen during scanning. Image reconstruction algorithms [27] and relative performance with different pinhole collimator materials [28] have been studied for this system using simulations. This paper presents the description and experimental performance characterization of the EXIRAD-3D technology using various phantom scans and mouse knee joint, thyroid, and kidney scans.

2. Materials and methods

2.1. System and collimator description

The EXIRAD-3D option uses a specially designed focusing multi-pinhole collimator which can be mounted on a U-SPECT/CT or a VECTor/CT imaging system (e.g. [29,30], MILabs B.V., The Netherlands). The system used in the present paper is equipped with three large-field-of-view gamma-cameras with 9.5 mm thick continuous NaI(Tl) crystals, each read out by 55 photomultiplier tubes. These gamma cameras attain a 3.5 mm intrinsic spatial resolution and 10% energy resolution at an energy of 140 keV. The cylindrical EXIRAD collimator contains 87 round pinholes (pinhole diameter 0.15 mm) with an inner collimator diameter of 21 mm. It is surrounded by a lead shielding tube with trapezium-shaped holes to prevent overlapping between pinhole projections on the detector (Fig. 1a). All pinhole axes converge at a single point in the collimator's center and together observe a field of view (FOV) with an hourglass shape with a diameter of 21 mm and a length of 13 mm. Note that the FOV can easily be extended several times longitudinally by stepping the object through the collimator with the scanning focus method [31] in which all projection data of the different object's positions are used simultaneously in image reconstruction.

Next to the new collimator, a specialized aluminum sample holder equipped with a cryo-cooling unit (Fig. 1b) was introduced to this system to keep tissue frozen in order to avoid activity leaking or tissue deformation during the scan. The cooling unit has a refillable chamber containing dry ice that maintains cryogenic temperature at the sample. Additionally, the robotic arm attached to the sample holder was improved for precise tissue placement inside the scanner during the scan and for accurate point source measurements for system calibration to guarantee the micro-scale image resolution.

2.2. Image reconstruction and processing

Calibration of EXIRAD-3D was done using a set of 435 ^{99m}Tc point source measurements, from which a full system matrix was generated using a model-based interpolation method [32] which is commonly used to generate system matrices for all SPECT collimators used on the U-SPECT/CT systems. For these measurements, a tiny point source is

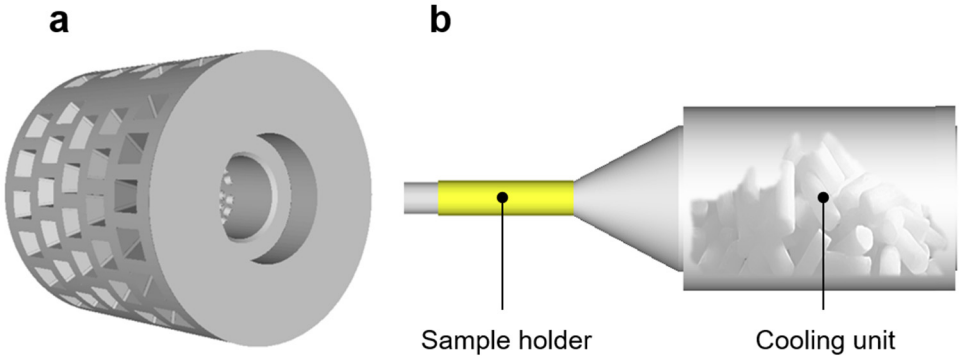

Fig. 1. (a) The focusing multi-knife-edge-pinhole collimator surrounded by the shielding tube with trapezium-shaped holes. (b) The cylindrical sample holder equipped with a cooling unit containing dry ice.

desirable (ideally a point); however, it is challenging to contain a large amount of radioactivity in a small volume. For the high-resolution EXIRAD-3D, we fabricated a 100-μm-diameter spherical point source, and were able to condense a 80 MBq activity of ^{99m}Tc in this source.

List-mode projection data were acquired for all scans with a ± 12.5% photopeak window centered at either 140 keV for ^{99m}Tc or 159 keV for ^{123}I. A similarity-regulated ordered-subset expectation maximization algorithm [33] with a maximum of 128 subsets was used for image reconstruction, except for the mouse knee joint scan where a pixel-based ordered-subset expectation maximization algorithm [34] with four subsets was used. Images were reconstructed on a 0.05 mm voxel grid using 20 iterations. Scatter and background radiation were corrected for using a triple-energy window method [35]. To this end, two side windows having a width of 20% of the photopeak window's width were placed adjacent to the photopeak. Gaussian and/or median post-filtering was applied to the reconstructed images with the filter size optimized manually for each scan (indicated below). The images in the Results section were displayed with a slice thickness of 0.2 mm except for the mouse knee joint scan where the slice thickness was 0.05 mm.

2.3. Experiments

The performance of EXIRAD-3D was characterized by scanning a Derenzo phantom to measure the system's resolution, a syringe phantom to show the system's uniformity and linearity, and several mouse tissues to illustrate which anatomical detail can be seen. The mouse experiments were performed with C57BL/6 mice under protocols approved by the Animal Research Committee at UMC Utrecht and in accordance with the Dutch Law on Animal Experimentation. The dissected tissue was snap-frozen in liquid nitrogen (except for the mouse knee joint) and subsequently placed inside the aluminum holder filled with Tissue-Tek OCT compound (Sakura Finetek Europe, cat. no. 4583) and attached to the cooler to keep the tissue frozen for the whole scan duration. Activity levels prior to the scans were measured using a dose calibrator (VDC-304, Veenstra Instruments, the Netherlands).

2.3.1. Phantom studies

System sensitivity was measured with a ^{99m}Tc point source placed at the collimator's center to calculate the ratio of the count rate (cps) within the acquisition window and the point source's activity (MBq).

System resolution was evaluated by scanning a Derenzo phantom having hot rods arranged in six sectors with rod diameters of 0.17, 0.16, 0.15, 0.14, 0.13, and 0.12 mm and a length of 1.5 mm. In each sector of this phantom, the distance between the centers of two adjacent rods is twice the rods' diameter. The resolution was defined as the diameter of the smallest rods that can be visually distinguished in the reconstructed image. The Derenzo phantom was filled with 4.06 MBq ^{99m}Tc-pertechnetate and scanned for 3 h. Images were reconstructed with 100% and 20% of the counts from the list-mode data to emulate the image resolution with the same scan time but with 100% and 20% of the initial radioactivity, respectively. A post-reconstruction 3D Gaussian filter having the full-width-at-half-maximum (FWHM) of 0.12 mm and 0.14 mm was applied on the 100%- and 20%-activity images, respectively.

The uniformity of the reconstructed images was assessed with a cylindrical phantom (inner diameter 8.5 mm, inner length 9.5 mm) filled with 38.6 MBq ^{99m}Tc-pertechnetate and scanned for 3 h. Images were reconstructed with 100%, 50%, and 20% of counts from the list-mode data to emulate the image uniformity with the same scan time but with 100%, 50%, and 20% of the initial radioactivity, respectively. A post-reconstruction 3D Gaussian filter having the FWHM of 0.6 mm was applied. To calculate the uniformity, nine regions of interest (ROIs), each formed by a circular disk with 3-mm radius and 0.3-mm thickness, were evenly placed on the image at 0.45-mm intervals. The uniformity was calculated as the ratio of the standard deviation between the ROIs' means to the average values from the ROIs, and represented as percentage.

Relative quantification was investigated with the same uniform phantom to see if the reconstructed image intensity changes linearly with activity.

2.3.2. Mouse knee joint scan

A mouse was anaesthetized with isoflurane and injected intravenously via the tail vein with 550 MBq technetium-99m methylene diphosphonate ([^{99m}Tc]MDP). Five hours post-injection, the mouse was euthanized and one of its limbs was excised and measured to contain 6 MBq activity at the start of the scan. The acquisition lasted for 7 h with 60-min time frames, focusing on the knee joint. The reconstructed SPECT image was post-filtered with a 0.1-mm-FWHM 3D Gaussian kernel. The knee joint was subsequently scanned in the CT module with a 4 μm resolution setting.

2.3.3. Mouse thyroid scan

A second mouse was anaesthetized with isoflurane and injected intravenously via the tail vein with 10.25 MBq [^{123}I]NaI. Four hours post-injection, the mouse was euthanized and a tissue volume containing the thyroid and a part of the trachea was excised and frozen as described above. The tissue was scanned for 11 h with 15 min time frames. A 0.15-mm-FWHM 3D Gaussian filter followed by a 3x3x3 median filter was applied to the reconstructed image.

2.3.4. Mouse kidney scan

A third mouse was injected intravenously via the tail vein with 75 MBq technetium-99m dimercaptosuccinic acid ([^{99m}Tc]DMSA). Three hours post-injection, the mouse was euthanized and one of its kidneys was excised and frozen as described above. The kidney was

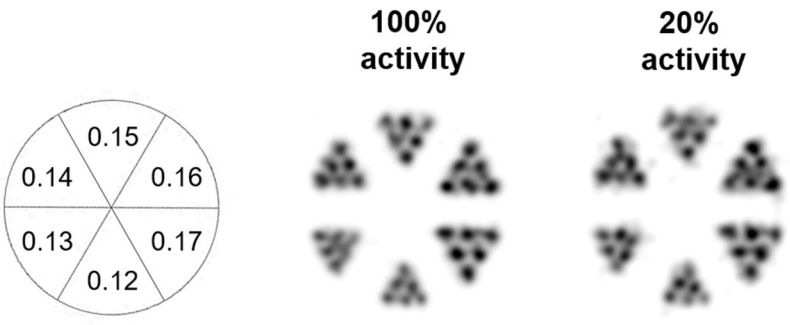

Fig. 2. Derenzo phantom scan with 4.06 MBq ^{99m}Tc-pertechnetate at the start and a scan time of 3 h. The images were reconstructed with 100% and 20% of the counts to emulate scans with the same scan time but with 100% and 20% of the initial activity. The rod diameters are provided in mm. Slice thickness was 0.2 mm.

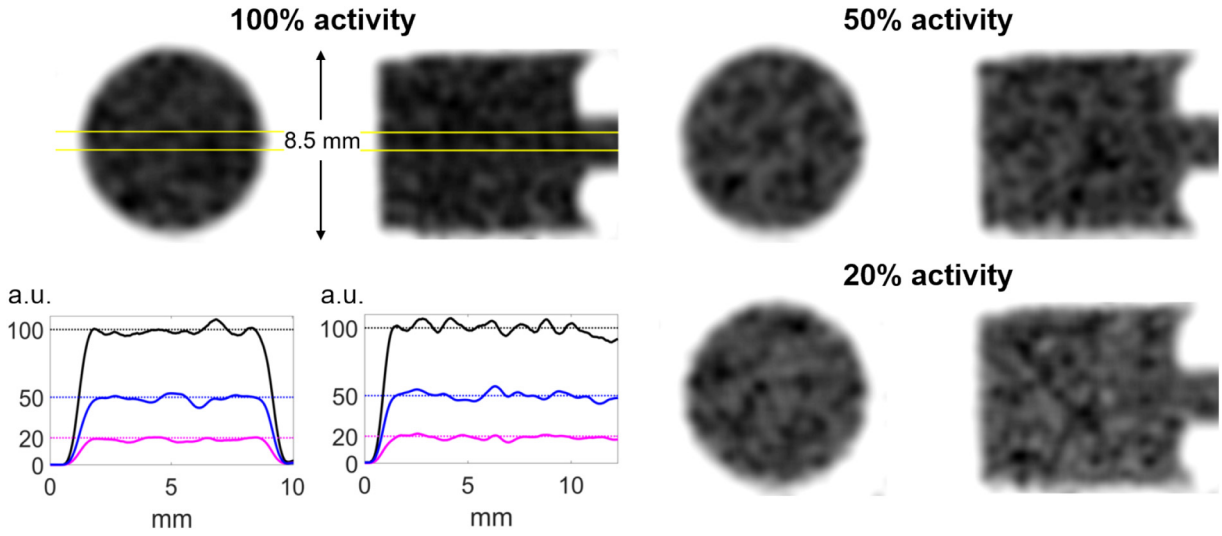

Fig. 3. Uniform phantom scan with 38.6 MBq ^{99m}Tc-pertechnetate at the start and a scan time of 3 h. The images were reconstructed with 100%, 50%, and 20% of the counts to emulate scans with the same scan time but with 100%, 50%, and 20% of the initial activity. For each reconstructed image, two perpendicular slices with a thickness of 0.2 mm are shown with gray scales in which white represents zero activity and black represents the maximum activity. Line profiles are also drawn at the position indicated with yellow lines on each slice. Here, the profiles are scaled by the same factor such that the average intensity within the phantom on the image reconstructed with 100% counts is 100.

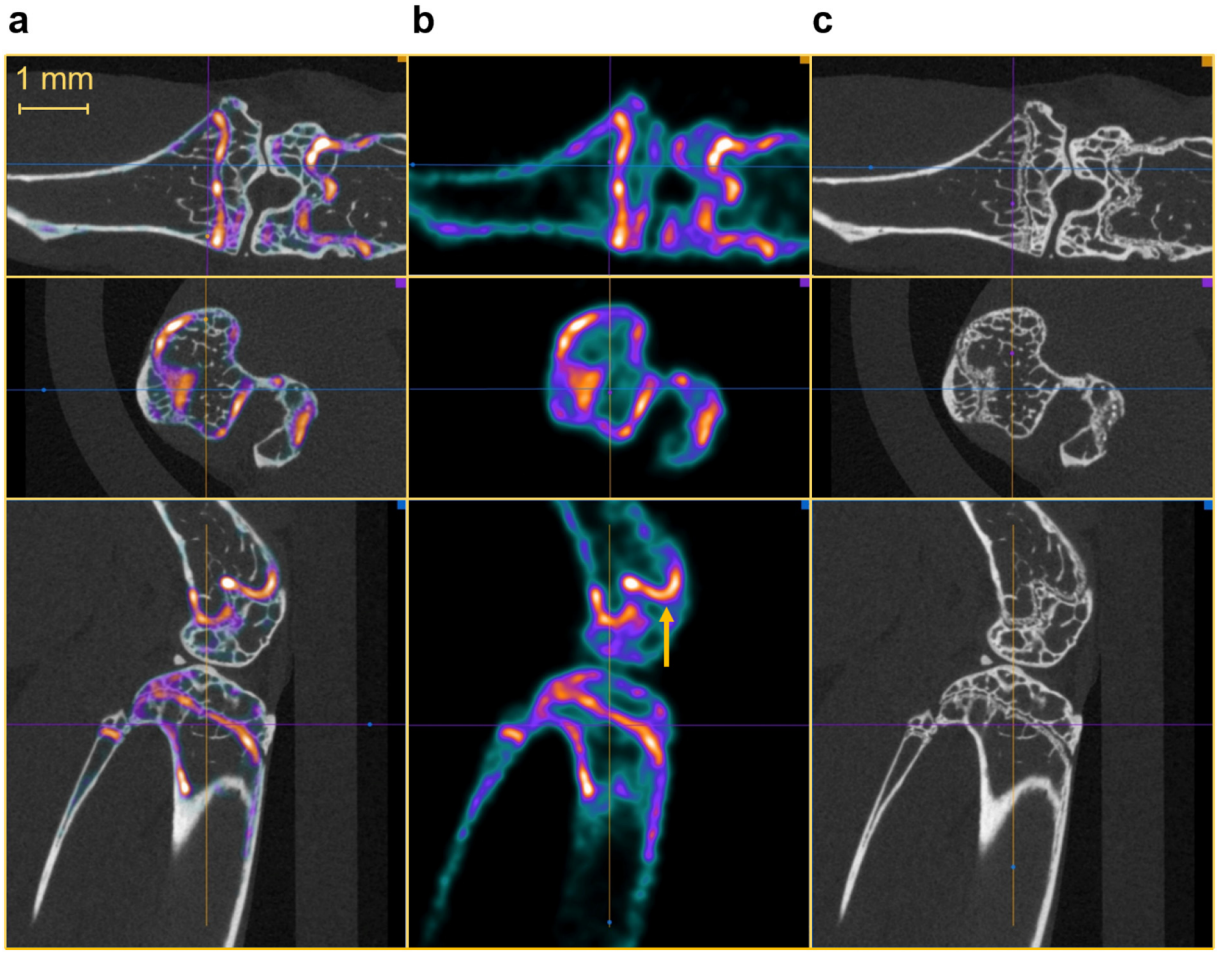

Fig. 4. (a) EXIRAD-3D SPECT images of [^{99m}Tc]MDP distribution in a mouse knee joint fused with CT. (b) Only the [^{99m}Tc]MDP SPECT images. The knee joint was measured to contain 6 MBq activity at the start, and the scan lasted for 7 h. Slice thickness was 0.05 mm. The arrow points at the activity distribution near the epicondylus lateralis of the knee joint. (c) Only the CT images obtained with the CT module on the same system and with a 4 μm resolution setting.

scanned for 11 h with 15 min time frames. A 0.28-mm-FWHM 3D Gaussian filter was applied to the reconstructed image.

3. Results

3.1. Phantom studies

The system sensitivity for ^{99m}Tc was determined to be 800 cps/MBq (or 0.08%) at the collimator's center. Fig. 2 shows an image of the Derenzo phantom reconstructed with two activity levels to test EXIRAD's spatial resolution. All rods in this phantom are discernable on the reconstructed images for both 100% and 20% of the activity, demonstrating a spatial resolution <120 μm (or 1.7 nl). This is about a ten times better volumetric resolution than that of state-of-the-art preclinical in vivo SPECT (250 μm, or 15.6 nl) [24].

Fig. 3 presents 0.2 mm thick slices of the uniform phantom images reconstructed with three activity levels and line profiles extracted from these slices at the positions indicated with yellow lines. The uniformity was 1.31%, 2.33%, and 3.01% for 100%, 50%, and 20% activity, respectively. The line profiles show that the reconstructed image intensity changes linearly as the activity varies, which shows the relative quantification result with this scanner.

3.2. Mouse knee joint scan

[^{99m}Tc]MDP labels sites of active bone turnover – the continuing process of bone resorption and formation taking place at a low physiological level. Fig. 4 shows three cross-sections of EXIRAD-3D SPECT and CT as well as the fused SPECT/CT through the mouse knee joint with [^{99m}Tc]MDP. Tiny details of bone turnover on many structures in the knee joint are visualized on the SPECT image, and the fused SPECT/CT image shows an excellent correlation of the [^{99m}Tc]MDP distribution to the anatomical microstructures on the CT image. Compared to in vivo bone knee scans with state-of-the-art 250-micron-resolution in vivo SPECT [24], much more detail was visible with EXIRAD-3D. For example, the tiny activity distribution near the epicondylus lateralis of the knee joint (see the arrow in Fig. 4) is clearly visualized with EXIRAD-3D while it is much more blurred with in vivo SPECT.

3.3. Mouse thyroid scan

Fig. 5a presents 3D views of the thyroid gland imaged using [^{123}I]NaI, and Fig. 5b shows coronal and axial slices through the thyroid. The two thyroid lobes are nicely visualized including the thin isthmus (also having iodine uptake) connecting the two lobes inferiorly and medially. As measured on the reconstructed image, each lobe is approximately 2.5 mm long, 1.3 mm wide, and 0.6 mm deep, and the isthmus is about 0.3 mm thin. The indents seen on the medial aspect of the two lobes as indicated in Fig. 5a (superior view) are corresponding to the thyroid part that wraps around the trachea near the base of the laryngeal cartilages. These anatomical details of the thyroid gland are in good agreement with the mouse atlas in [36].

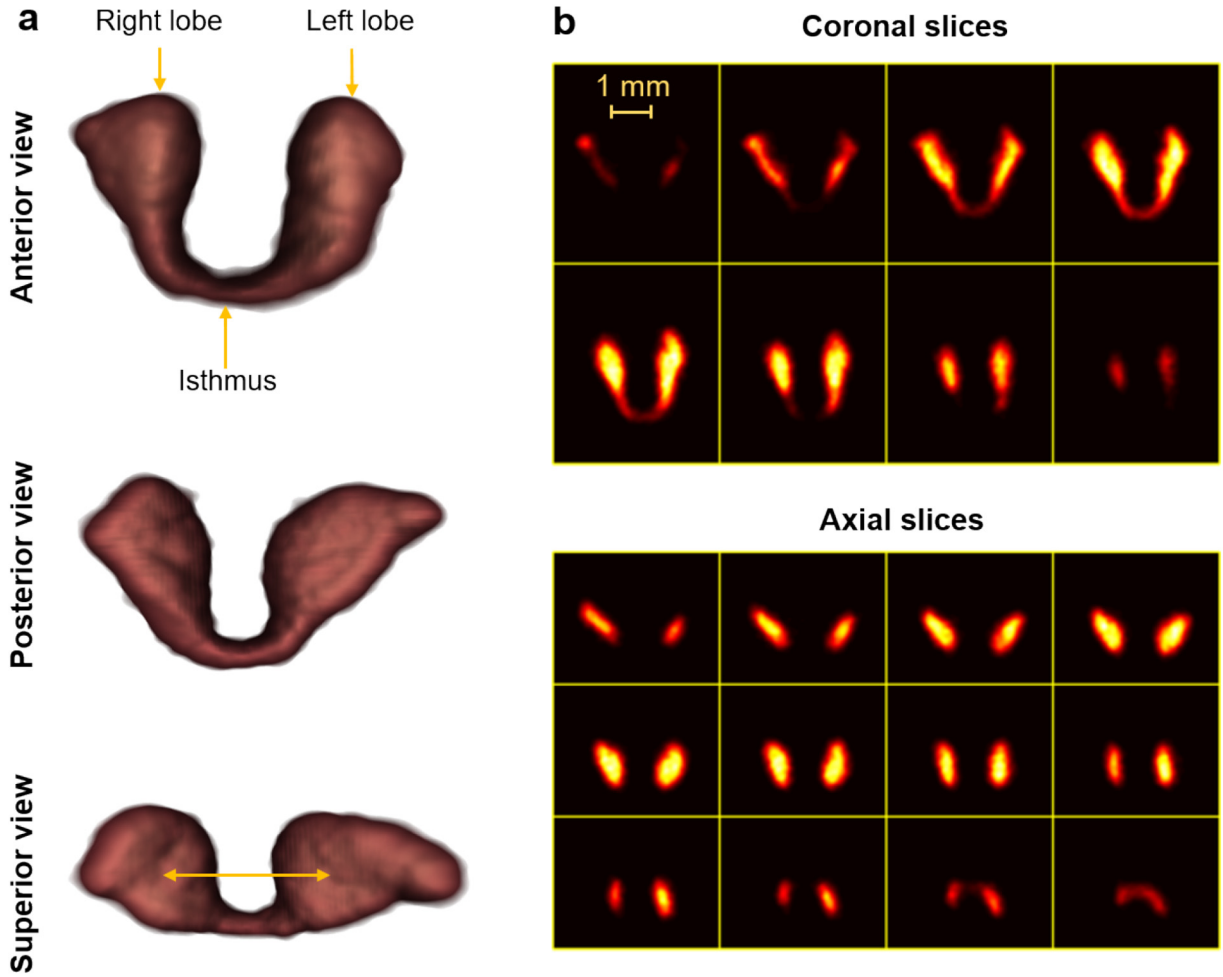

Fig. 5. [^{123}I]NaI scan of the mouse thyroid with 10.25 MBq activity injected intravenously and a scan time of 11 h. (a) 3D anterior, posterior, and superior views of the reconstructed thyroid. (b) Selected coronal and axial slices through the thyroid. Slice thickness was 0.2 mm.

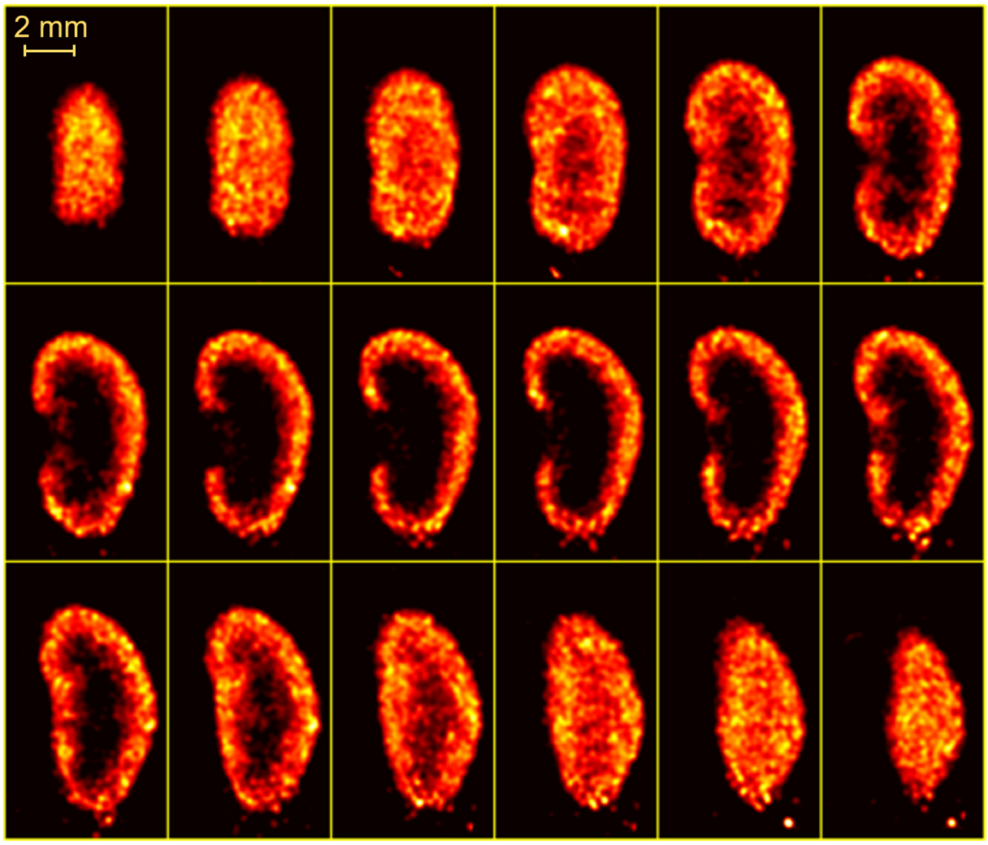

Fig. 6. [^{99m}Tc]DMSA scan of the mouse kidney with 75 MBq activity injected intravenously and a scan time of 11 h. Slice thickness was 0.2 mm.

3.4. Mouse kidney scan

Fig. 6 shows slices through the [^{99m}Tc]DMSA kidney image obtained ex vivo using EXIRAD-3D. As anticipated, the [^{99m}Tc]DMSA tracer distribution is revealed in the renal cortex but not in the medullar cavity. Some structures on the renal cortex (higher-uptake areas), which are believed to be corresponding to the parts of nephrons, are also visualized. The small amount of activity seen outside the kidney at the bottom of the image is probably because of the tissue handling process in which activity on the tools may end up in the Tissue-Tek compound when placing the sample into the holder.

4. Discussion

We presented a fast automated three-dimensional autoradiography technique capable of imaging radiolabeled molecule distributions in tissue samples at a resolution of 120 μm. This technique is enabled using a specialized focusing multi-pinhole collimator mounted on a U-SPECT/CT system and a built-in cryo-cooling unit. Because of the close distance between the pinholes and the tissue volume and large pinhole magnification factors, high-resolution 3D images can be obtained. Furthermore, as described in the Method section, EXIRAD-3D has some other significant adaptations compared to U-SPECT/CT which together translate into substantial improvement in image quality: (i) a novel specialized cryo-cooling unit to keep tissue frozen during the scan that has not been used in any prior preclinical SPECT system, (ii) a more precise robotic arm for accurate tissue and point source placement, and (iii) a considerable effort invested in system calibration to address the challenge posed by the small point source size.

With EXIRAD-3D, the imaging volume can be easily adjusted using a patented acquisition interface and a highly focused scan is accomplishable [31]. Since a more focused scan means that more counts can be acquired from the volume of interest in a given time that benefits the image quality, we recommend using EXIRAD-3D in the highest possible focusing mode. In other words, the selected scan volume should be set just large enough to cover the tissue sample. The system resolution can be possibly improved for higher-energy isotopes by employing pinhole inserts made of a material with higher photon-stopping power than tungsten such as gold or gold-platinum alloy, as previously studied in [28]. In addition, extending the scan time could enhance the image quality even further, provided of course that the isotope's half-life is sufficiently long. This is practical as in such long scans, the tissue is kept frozen to immobilize the activity distribution, and thus scans can be done overnight without an operator present.

In this work, we have presented quantitative results showing that the reconstructed activity scales linearly with the real activity on the phantom. In order to obtain absolute quantification (i.e. the activity concentration in terms of MBq/ml) the method presented in [37] can be applied for ex vivo scans in the same way as for in vivo scans with our systems. In this case, the reconstructed image is simply scaled by a calibration coefficient defined as the ratio of the activity concentration to the voxel value in reconstructed images, which is obtained by scanning a point source with known activity of a studied isotope and then applying it to all scans done with that isotope and the same system settings.

Despite the listed limitations of traditional autoradiography, it is currently still common practice when a very high resolution at the cellular level is desired. Besides, traditional autoradiography can also image pure alpha- and beta-emitters while this is not an option with the current EXIRAD-3D that is only designed for imaging gamma-emitters. However, EXIRAD-3D (with 1.7 nl volumetric resolution) has reached the resolution range of autoradiography (from 0.01 pl to several nl, [38]), and it can, for a subset of these studies, be a good alternative for traditional autoradiography, in particular as an option on a U-SPECT/CT or a VECTor/CT imaging system that facilitates longitudinal studies on the same animal, and provides a direct link between in vivo and ex vivo datasets. The increase in resolution and user convenience are

achieved with little additional effort instead of going through the complicated tissue sectioning process with completely different autoradiography laboratory equipment. With EXIRAD-3D, the only additions to the common in vivo workflow are dissection of the organs and snap-freezing them. The latter takes less than 10 min for e.g. the thyroid. The complexity of tissue dissection depends on the studied tissue, but it is much less labor intensive than performing traditional autoradiography in 3D.

5. Conclusion

This paper characterized the performance of EXIRAD-3D as a new technique for autoradiography. Phantom scans demonstrated 120 μm spatial resolution, and ex vivo mouse tissue scans visualized tiny details of the mouse knee joint, thyroid, and kidney. The acquired 3D autoradiographs can be perfectly overlaid with ultra-high resolution CT images and directly linked to the in vivo results obtained in a multimodal acquisition with the same platform, e.g. after a longitudinal imaging study.

Declaration of competing interests

Freek J. Beekman is a founder, shareholder, and part-time board member of MILabs. Ruud M. Ramakers, Chris Kamphuis, and Sofia Koustoulidou are employees of MILabs. No other potential competing interests relevant to this article was reported.

Credit authorship contribution statement

Minh Phuong Nguyen: Methodology, Writing - original draft, Writing - review & editing. **Ruud M. Ramakers:** Methodology, Writing - review & editing. **Chris Kamphuis:** Writing - review & editing, Methodology, Software. **Sofia Koustoulidou:** Methodology, Writing - review & editing. **Marlies C. Goorden:** Supervision, Writing - review & editing. **Freek J. Beekman:** Supervision, Writing - review & editing.

References

[1] Appleton TC. Autoradiography of soluble labelled compounds. J R Microsc Soc. 1964; 83:277–81.
[2] Ullberg S. The technique of whole body autoradiography : cryosectioning of large specimens. Sci Tools. 1977:2–29.
[3] Solon EG. Autoradiography techniques and quantification of drug distribution. Cell Tissue Res. 2015;360:87–107.
[4] McEwen A, Henson Cl. Quantitative whole-body autoradiography: past, present and future. Bioanalysis. 2015;7:557–68.
[5] Zhao W, Young TY, Ginsberg MD. Registration and three-dimensional reconstruction of autoradiographic images by the disparity analysis method. IEEE Trans Med Imaging. 1993;12(4):782–91.
[6] Kim B, Boes JL, Frey KA, Meyer CR. Mutual information for automated unwarping of rat brain autoradiographs. Neuroimage. 1997;5:31–40.
[7] Rangarajan A, Chui H, Mjolsness E, et al. A robust point-matching algorithm for autoradiograph alignment. Med Image Anal. 1997;1:379–98.
[8] Barthe N, Chatti K, Coulon P, Maîtrejean S, Basse-Cathalinat B. Recent technologic developments on high-resolution beta imaging systems for quantitative autoradiography and double labeling applications. Nucl Instruments Methods Phys Res Sect A Accel Spectrometers, Detect Assoc Equip. 2004;527:41–5.
[9] Karellas A, Liu H, Reinhardt C, Harris LJ, Brill AB. Imaging of radionuclide emissions with a low-noise charge-coupled device. IEEE Trans Nucl Sci. 1993;40:979–82.
[10] Laniece P, Charon Y, Cardona A, et al. A new high resolution radioimager for the quantitative analysis of radiolabelled molecules in tissue section. J Neurosci Methods. 1998;86:1–5.
[11] Cabello J, Bailey A, Kitchen I. The performance of a CCD digital autoradiography imaging system. Phys Med Biol. 2000;45:2011.
[12] Kokkinou E, Wells K, Petrou M, Bailey A. Digital autoradiography imaging using direct irradiation of a CCD between 278-309 K. 2002 IEEE nuclear science symposium conference record. IEEE; 2003. p. 1607–11.
[13] Peng Q, Holland SE, Choong WS, Budinger TF, Moses WW. Real-time quantitative ex vivo direct autoradiography with 10μm pixel resolution. 2011 annual international conference of the IEEE engineering in medicine and biology society. IEEE; 2011. p. 6273–6.
[14] Montesi MC. BETAview autoradiography system: laboratory tests and biological experiments. Nucl Instruments Methods Phys Res Sect A Accel Spectrometers, Detect Assoc Equip. 2001;461:425–7.
[15] Mettivier G, Montesi MC, Russo P. Digital autoradiography with a Medipix2 hybrid silicon pixel detector. IEEE Trans Nucl Sci. 2005;52:46–50.
[16] Russo P, Lauria A, Mettivier G, et al. 18 F-FDG positron autoradiography with a particle counting silicon pixel detector. Phys Med Biol. 2008;53:6227–43.
[17] Cabello J, Esposito M, Mettivier G, et al. Digital autoradiography using room temperature CCD and CMOS imaging technology. Phys Med Biol. 2007;52:4993.
[18] Nguyen Pham T, Finck C, Marchand P, Brasse D, Boisson F, Laquerriere P. 18F autoradiography using pixelated CMOS technology. Proc - 2017 IEEE 15th Int New Circuits Syst Conf NEWCAS 2017; 2017. p. 41–4.
[19] Ulrici J, Fischer P, Klein P, et al. Imaging performance of a DEPFET pixel bioscope system in tritium autoradiography. Nucl Instruments Methods Phys Res Sect A Accel Spectrometers, Detect Assoc Equip. 2005;547:424–36.
[20] Bertolucci E, Conti M, Grossi G, et al. Autoradiography with silicon strip detectors. Nucl Instruments Methods Phys Res Sect A Accel Spectrometers, Detect Assoc Equip. 1996;381:527–30.
[21] Lees JE, Pearson JF, Fraser GW, Hales JM, Richards PG. An mcp-based system for beta autoradiography. IEEE Trans Nucl Sci. 1999;46:636–8.
[22] Lees JE, Murray A, Perkins AC, Fraser GW. Autoradiography of high-energy radionuclides using a microchannel plate detector. IEEE Trans Nucl Sci. 2002;49:153–5.
[23] Dooraghi AA, Vu NT, Silverman RW, et al. Betabox: a beta particle imaging system based on a position sensitive avalanche photodiode. Phys Med Biol. 2013;58: 3739–53.
[24] Ivashchenko O, van der Have F, Villena JL, et al. Quarter-millimeter-resolution molecular mouse imaging with U-SPECT^{+}. Mol Imaging. 2014;13.
[25] Meng L-J, Tan JW, Fu G, et al. An ultra-high resolution SPECT/CT system for 3-D autoradiography. J Nucl Med. 2007;48:459P.
[26] Ramakers R, Vastenhouw B, Beekman F. Ultra-high resolution cardiac SPECT of frozen animals as an alternative to autoradiography. , vol 50Society of Nuclear Medicine; 2009.
[27] Nguyen MP, Ensing W, Vastenhouw B, et al. System modeling and image reconstruction for 3D micron-resolution autoradiography. *NSS-MIC*; 2017.
[28] Nguyen MP, Goorden MC, Kamphuis C, Beekman FJ. Evaluation of pinhole collimator materials for micron-resolution ex vivo SPECT. Phys Med Biol. 2019;64.
[29] van der Have F, Vastenhouw B, Ramakers RM, et al. U-SPECT-II: an ultra-high-resolution device for molecular small-animal imaging. J Nucl Med. 2009;50: 599–605.
[30] Goorden MC, van der Have F, Kreuger R, et al. VECTor: a preclinical imaging system for simultaneous submillimeter SPECT and PET. J Nucl Med. 2013;54:306–12.
[31] Branderhorst W, Vastenhouw B, Van Der Have F, Blezer ELA, Bleeker WK, Beekman FJ. Targeted multi-pinhole SPECT. Eur J Nucl Med Mol Imaging. 2011;38:552–61.
[32] van der Have F, Vastenhouw B, Rentmeester M, Beekman FJ. System calibration and statistical image reconstruction for ultra-high resolution stationary pinhole SPECT. IEEE Trans Med Imaging. 2008;27:960–71.
[33] Vaissier PEB, Beekman FJ, Goorden MC. Similarity-regulation of OS-EM for accelerated SPECT reconstruction. Phys Med Biol. 2016;61:4300–15.
[34] Branderhorst W, Vastenhouw B, Beekman FJ. Pixel-based subsets for rapid multi-pinhole SPECT reconstruction. Phys Med Biol. 2010;55:2023–34.
[35] Ogawa K, Harata Y, Ichihara T, Kubo A, Hashimoto S. A practical method for position-dependent Compton-scatter correction in single photon emission CT. IEEE Trans Med Imaging. 1991;10:408–12.
[36] Treuting PM, Dintzis SM. Comparative anatomy and histology: A mouse and human atlas. Academic; 2012.
[37] Wu C, Van Der Have F, Vastenhouw B, Dierckx RAJO, Paans AMJ, Beekman FJ. Absolute quantitative total-body small-animal SPECT with focusing pinholes. Eur J Nucl Med Mol Imaging. 2010;37:2127–35.
[38] Hargreaves R, Hoppin J, Sevigny J, et al. Optimizing central nervous system drug development using molecular imaging. Clin Pharmacol Ther. 2015;98:47–60.